



HAL
open science

Minibeam radiation therapy at a conventional irradiator: Dose-calculation engine and first tumor-bearing animals irradiation

W. González, M. dos Santos, C. Guardiola, R. Delorme, C. Lamirault, M. Juchaux, M. Le Dudal, G. Jouvion, Y. Prezado

► To cite this version:

W. González, M. dos Santos, C. Guardiola, R. Delorme, C. Lamirault, et al.. Minibeam radiation therapy at a conventional irradiator: Dose-calculation engine and first tumor-bearing animals irradiation. *Physica Medica*, 2020, 69, pp.256-261. 10.1016/j.ejmp.2019.12.016 . hal-02447924

HAL Id: hal-02447924

<https://hal.science/hal-02447924>

Submitted on 20 Aug 2020

HAL is a multi-disciplinary open access archive for the deposit and dissemination of scientific research documents, whether they are published or not. The documents may come from teaching and research institutions in France or abroad, or from public or private research centers.

L'archive ouverte pluridisciplinaire **HAL**, est destinée au dépôt et à la diffusion de documents scientifiques de niveau recherche, publiés ou non, émanant des établissements d'enseignement et de recherche français ou étrangers, des laboratoires publics ou privés.

1 Minibeam radiation therapy at a conventional irradiator: Dose- 2 calculation engine and first tumor-bearing animals irradiation 3

4 W. González¹, M. dos Santos¹, C. Guardiola¹, R. Delorme¹, C. Lamirault¹, M. Juchaux¹, M. Le Dudal^{2,3}, G.
5 Jouvion^{2,4}, Y. Prezado^{1,*}

6 ¹ *IMNC-UMR 8165, CNRS, Paris 7 and Paris 11 Universities, 15 rue Georges Clemenceau, 91406 Orsay*
7 *Cedex, France*

8 ² *Institut Pasteur, Experimental Neuropathology Unit, Department of Global Health, 75015 Paris, France*

9 ³ *Histologie, Embryologie et Anatomie Pathologique, Ecole Nationale Vétérinaire d'Alfort, Université Paris-*
10 *Est, Maisons-Alfort, France*

11 ⁴ *Sorbonne Université, INSERM, Physiopathologie des Maladies Génétiques d'Expression Pédiatrique,*
12 *Assistance Publique des Hôpitaux de Paris, Hôpital Armand-Trousseau, UF de Génétique Moléculaire, Paris,*
13 *France*

14 * *Corresponding author. E-mail address: prezado@gmail.com*

15 16 Abstract:

17 Purpose: Minibeam radiation therapy (MBRT) is a novel therapeutic strategy, whose exploration was
18 hindered due to its restriction to large synchrotrons. Our recent implementation of MBRT in a wide-spread
19 small animal irradiator offers the possibility of performing systematic radiobiological studies. The aim of
20 this research was to develop a set of dosimetric tools to reliably guide biological experiments in the
21 irradiator.

22 Methods: A Monte Carlo (Geant4)-based dose calculation engine was developed. It was then benchmarked
23 against a series of dosimetric measurements performed with gafchromic films. Two voxelized rat
24 phantoms (ROBY, computer tomography) were used to evaluate the treatment plan of F98 tumor-bearing
25 rats. The response of a group of 7 animals receiving a unilateral irradiation of 58 Gy was compared to a
26 group of nonirradiated controls.

27 Results: The good agreement between calculations and the experimental data allowed the validation of
28 the dose-calculation engine. The latter was first used to compare the dose distributions in computer
29 tomography images of a rat's head and in a digital model of a rat's head (ROBY), obtaining a good general

30 agreement. Finally, with respect to the in vivo experiment, the increase of mean survival time of the
31 treated group with respect to the controls was modest but statistically significant.

32 Conclusions: The developed dosimetric tools were used to reliably guide the first MBRT treatments of
33 intracranial glioma-bearing rats outside synchrotrons. The significant tumor response obtained with
34 respect to the non-irradiated controls, despite the heterogenous dose coverage of the target, might
35 indicate the participation of non-targeted effects.

36 *Keywords: X-ray Minibeam radiation therapy, Monte Carlo simulations, ROBY*

37 I. INTRODUCTION

38 Minibeam radiation therapy (MBRT) is an innovative tumor therapy that was initiated at synchrotrons [1].
39 The dose is spatially fractionated by summing submillimetric (500–700 μm) beams in a comb-like pattern:
40 the dose profiles consist of peaks and valleys with high doses in the beam path and low doses in the spaces
41 between them [2]. The peak-to-valley dose ratio (PVDR) is considered an important dosimetric parameter
42 [3], since in order to spare the normal tissues, high PVDR and low valley doses are required.

43 MBRT has been shown to increase normal tissue tolerances [4]. In addition, a significant delay in tumor
44 growth was observed in glioma bearing rats [5]. The extension of MBRT to contexts outside of synchrotron
45 biomedical beamlines towards a conventional irradiator would facilitate the realization of comprehensive
46 radiobiological studies [6]. For that purpose, we have modified a commercial X-ray small animal irradiator
47 to make it suitable for MBRT small animal irradiation [6]. This involves obtaining minibeam patterns with
48 comparable widths and PVDR values to those at synchrotrons. This strategy offers several advantages over
49 synchrotron radiotherapy (RT), such as reduced costs, and the possibility of envisioning clinical trials with
50 modified equipment, without the difficulties imposed by the scarce beam time at synchrotrons.

51 The aim of this research was to develop the necessary dosimetric tools to design, guide, and interpret
52 biological experiments. This included the development of a Monte Carlo-based dose calculation engine, to
53 guide and analyse small-animal MBRT experiments. Calculations in a voxelized rat brain, both using and
54 comparing an analytical phantom (ROBY) and computer tomography images of the rat to be treated, were
55 performed. The suitability of using ROBY in case computer tomography images (CT) of the animals are not
56 available, was established. The developed dosimetry tools were used to guide the first evaluation of the
57 effectiveness of tumor response in glioma-bearing rats outside synchrotron sources, which is also
58 reported. To the best of our knowledge, this is the first proof-of-concept of MBRT irradiation of intracranial
59 gliomas in rodents performed in a table-top system.

60 II. MATERIALS AND METHODS

61 a. Monte Carlo simulations

62 The implementation of the MBRT technique was carried out at the Small Animal Radiation Research
63 Platform (SARRP, XSTRAHL Ltd., UK) [7] available at the Experimental Radiotherapy Platform of the Curie
64 Institute in Orsay (France). The SARRP was modified to make it suitable for MBRT experiments [6]. The
65 SARPP can be used both for therapy and imaging. A small focal spot (1 mm diameter) leading to energies
66 around 60–70 kVp are used for imaging, while higher kV X-ray tension and a larger focal spot (5.5 mm
67 diameter) are used for irradiations. The collimator was designed to obtain beam widths and centre-to-
68 centre (ctc) distances comparable to those previously used at ESRF (600 μm width and 1200 μm ctc) [6].

69 Monte Carlo (MC) simulations were used to guide the design, setup optimization and to develop a Monte
70 Carlo-based dose calculation engine. The MC toolkit Geant4 version 10.01 [8] was employed. For all the
71 particles, a cut energy of 250 eV was considered. The Livermore electromagnetic physics list was used.

72 *i. Virtual source model*

73 A virtual source was defined to save computing time. For source definition, MC simulations were split into
74 two parts. First, electron interactions on the tungsten anode were simulated and the phase space variables
75 (particle type, energy, position, momentum) of the photon created, after passing through the inherent
76 and additional filtration of 0.8 mm of beryllium and 0.15 mm of copper, were saved into a phase space file
77 (PSF). The analysis of the information contained in this PSF was then used to generate a photon virtual
78 source model placed at the anode position of the SARRP. For fine tuning of the source, an iterative process
79 guided by the comparison of the simulated and measured dose distributions was followed. The energy
80 spectrum was determined by using the software SpekCalc [6].

81 The criteria of acceptability for the dose calculations compiled in the Technical Report Series 430 (TRS 430)
82 of the International Atomic Energy Agency [9] were considered.

83 The validated source model was then used as input for the subsequent dose calculations.

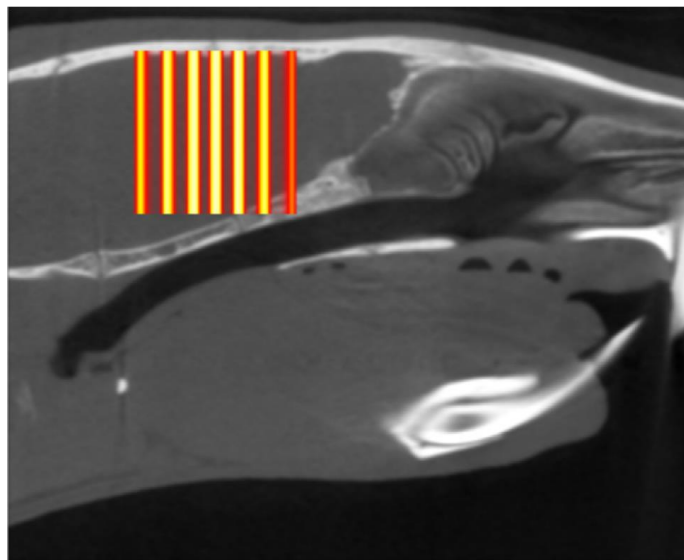
84 *ii. Dose calculation engine*

85 A Geant4-based dose engine (dose-engine) for X-ray MBRT was developed using the idea of the
86 manipulation of a voxelized phantom from the Geant4 extended example DICOM. The DICOM example
87 shows how to construct a geometry in Geant4 starting from the CT of real patient data [8].

88 The number of primary particles used in the simulations was 1011 so that the global uncertainty was 2%,
89 with a coverage factor $k = 1$. The dose was scored in voxels of $0.1 \times 0.1 \times 0.1 \text{ mm}^3$ in four different
90 phantoms. In order to speed up the calculation a nested parametrization was employed.

91 Two phantoms with dimensions of $200 \times 200 \times 40 \text{ mm}^3$, mimicking those used in the experimental
92 measurements, were considered. One of them was a homogenous solid water phantom (Gammex [10]).
93 It was used for comparison with the experimental dosimetry data to fine-tune the geometric
94 characteristics of the collimator, as well as to benchmark our dose-engine. The other one, a heterogeneous
95 phantom, consisting of a 10-mm thick slab of bone and three 10-mm thick slabs of solid water was
96 employed to validate the performance of the dose-engine in the presence of heterogeneities.

97 Two voxelized rat phantoms were used to plan the dosimetry of the radiotherapy treatment of the tumor
98 lesions on the head. The first one, called ROBY [11], is a digital model of the rat's whole body. Similar digital
99 phantom has been used in previous RT studies [12]. In this study, we only considered the slice of the ROBY
100 phantom representing the rat's head. The second phantom was composed of the CT images of a 7-week
101 old rat. The CT images were acquired using the SARRP. The reconstruction was done by filtered
102 Backprojection without post filtering. The Fig. 1 represent a sagittal section of the CT phantom including
103 the beam eye view of the arrangement projected over it.



104

105 *Fig. 1: Beam eye view image of the beam arrangement projected on a sagittal section of the CT phantom.*

106 Regarding the ROBY phantom, the attenuation coefficient table as a function of the energy was used to
107 generate the voxelized geometry. In our case, for each energy, the values of the attenuation coefficient

108 were replaced by the material's density. Using a customized precompilation routine, the raw output file
109 of ROBY was converted into 300 slices with dimensions of $55.3 \times 35.6 \times 0.1 \text{ mm}^3$.

110 Concerning the CT images, the conversion from Hounsfield units (HU) per pixel to material density was
111 performed following the steps described by Reynaert et al. [13]. Using the pre-compiled routine, 300 slices
112 with dimension $68.1 \times 41.1 \times 0.1 \text{ mm}^3$ were generated.

113 The dose distribution in the rats' brains in the in vivo experiment were assessed by using the developed
114 dose-engine.

115 A comparison between the dose distributions obtained in ROBY and in the rat's CT was performed to
116 evaluate whether ROBY could be used as a substitute to plan experiments. This could be convenient if the
117 sizes of the animals of the same group are not very homogeneous and there is no possibility of performing
118 high-resolution CT for each of the animals to be irradiated, a procedure that is very time consuming. The
119 advantage of ROBY is that the dimensions can be modified to be adapted to different ages/sizes of the rats
120 to be irradiated.

121 b. Experimental dosimetry

122 The experimental dosimetry was performed following the 'two-step' protocol developed for synchrotron
123 MBRT [2]. In this protocol, the reference dose (D_{ref}) is measured in a broad beam configuration with a
124 thimble ionization chamber (PTW PinPoint 31016 chamber). A reference field size of $40 \times 40 \text{ mm}^2$ was
125 chosen.

126 For relative dosimetry, radiochromic films (Gafchromic EBT3 films, Gafchromic™) were used. A flatbed
127 scanner (Epson Perfection V750-M Pro Scanner) served to readout the films, following the method
128 described in Devic et al. [14]. Film handling was carried out taking into account the recommendations
129 provided by Task Group 55 of the American Association of Physics in Medicine (AAPM) [15]. The
130 uncertainties of the film dose measurements were evaluated following the method described in Sorriaux
131 et al. [16]. The main contributions to the overall uncertainty come from the determination of the absolute
132 dose with the ionization chamber (2%), the measurement of the film's optical density (0.5%), film
133 calibration (1.5%), and the mean standard deviation of the average dose in the peak and valley regions
134 (2%). The overall uncertainty amounted to 3.2%. To incorporate other possible sources of uncertainty, a
135 conservative value of 4% was used.

136 The films were placed at different depths in two different plastic phantoms (Gammex [10]). The first one
137 was a solid water phantom consisting of 4 slabs with dimensions of $200 \times 200 \times 10 \text{ mm}^3$. The second one

138 was a heterogeneous phantom composed of 1 slab (200×200×10 mm³) of bone-equivalent material and 3
139 slabs of solid water.

140 Percentage depth dose curves and lateral dose profiles were measured. Finally, the output factors were
141 assessed by comparing the ratio of the dose measured by the films irradiated with a 40 × 40 mm² field
142 size and those irradiated with MBRT at different depths.

143 c. In vivo experiment

144 The dosimetry tools developed were used to guide the first evaluation of tumor response effectiveness in
145 glioma-bearing rats. The ethical guidelines of our institutions for animal welfare were followed in
146 conducting the experiments. They were approved by the Ethics Committee of the Institut Curie and the
147 French Ministry of Research (permit No. 6361-201608101234488).

148 A number of 10000 F98 rat cells (ATCC[®]CRL-2397[™]), transfected with the luciferase gene, were implanted
149 in male Fischer 344 rats (Janvier Labs). The cells were inoculated, as in our previous research [17].
150 Bioluminescence Imaging (BLI) at an IVIS spectrum (PerkerElmer) was carried out to confirm the presence
151 of a tumor. A double control was performed through a histopathological analysis when the animals died.

152 Two groups of animals (7 weeks old at the moment of irradiation) were considered: i) a control group
153 (tumor bearing rats, non-irradiated) (n = 4); ii) a group of tumor-bearing rats n = 7) that received MBRT.

154 The rats were irradiated 11 days after implantation. The irradiation was a lateral one from left to right. In
155 this irradiation configuration, the centre of the tumor was located at a depth of approximately 16 mm.
156 The dose delivered was 58 Gy (peak dose) as measured at 1 cm in depth in a water phantom. The goal was
157 to assess whether some tumor response is achieved with those high doses in MBRT.

158 The dose distributions in the rat's brain were calculated with the dose engine described in Section 2.1.2,
159 and will be presented in the Results section. The doses were delivered in only one fraction.

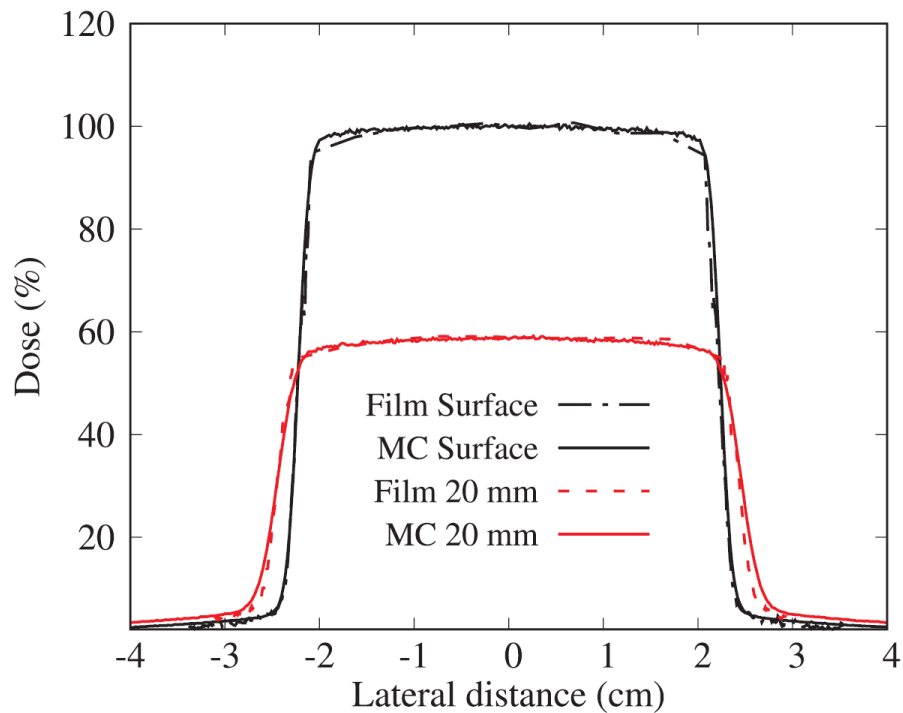
160 III. RESULTS

161 In this section we present the dose measurements, the benchmarking of the dose-engine, and the dose
162 calculations to plan the in vivo experiment. The results of this first evaluation of the effectiveness of MBRT
163 for glioma tumor response in a conventional irradiator will also be presented.

164 a. Dosimetry

165 As explained in the Methods section, a virtual source model placed at the anode position was extrapolated
166 from the dose distributions measured in standard conditions (seamless irradiation) by using an iterative
167 method. A Gaussian source with a full width at half maximum (FWHM) of 2.3 mm and a divergence of 20

168 degrees reproduced well the experimental data. Fig. 2 shows the transversal dose profiles for a seamless
169 irradiation ($40 \times 40 \text{ mm}^2$ field size).

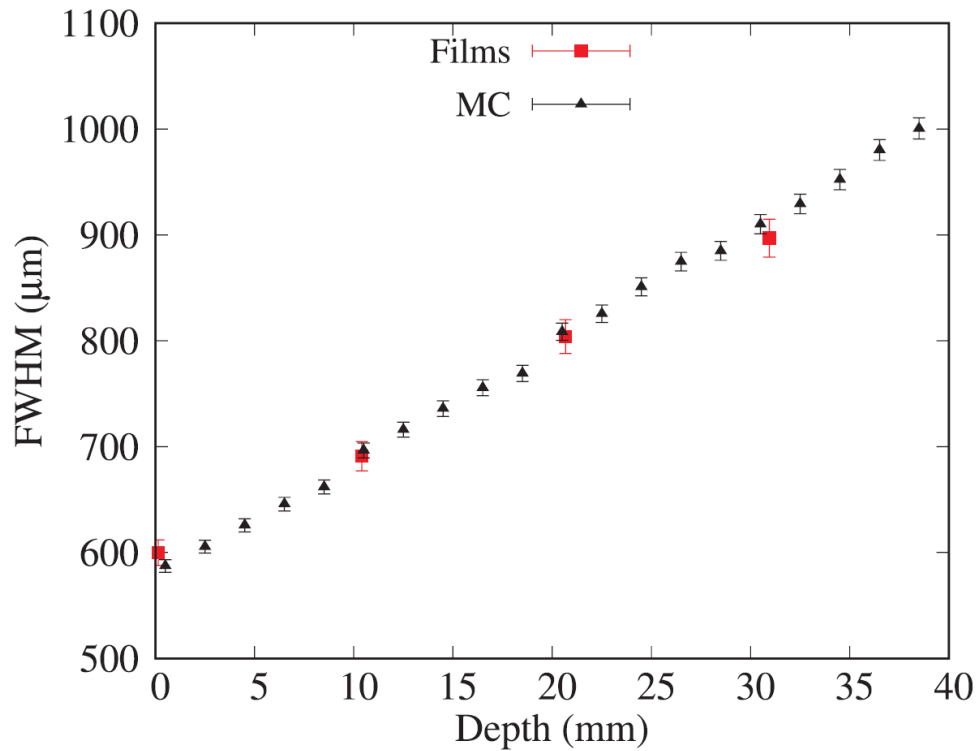


170

171 *Fig. 2: Comparison of experimental and calculated doses in broad beam configuration. Lateral dose profiles at surface and 20*
172 *mm of depth. The values were normalized to the maximum value.*

173 A good agreement between the MC simulations and the experimental data is observed, according to the
174 criteria explained in the TRS430 [9]. The relative differences around the maximum region of the transverse
175 dose profiles were 2% at most. The difference regarding the penumbra distances between simulated and
176 experimental profiles was smaller than 1.2 mm.

177 By using the validated source model, the dose distributions in both the homogeneous and heterogeneous
178 solid phantoms were assessed. Fig. 3 depicts the FWHM of the central peak of the MBRT array in the
179 homogeneous configuration.

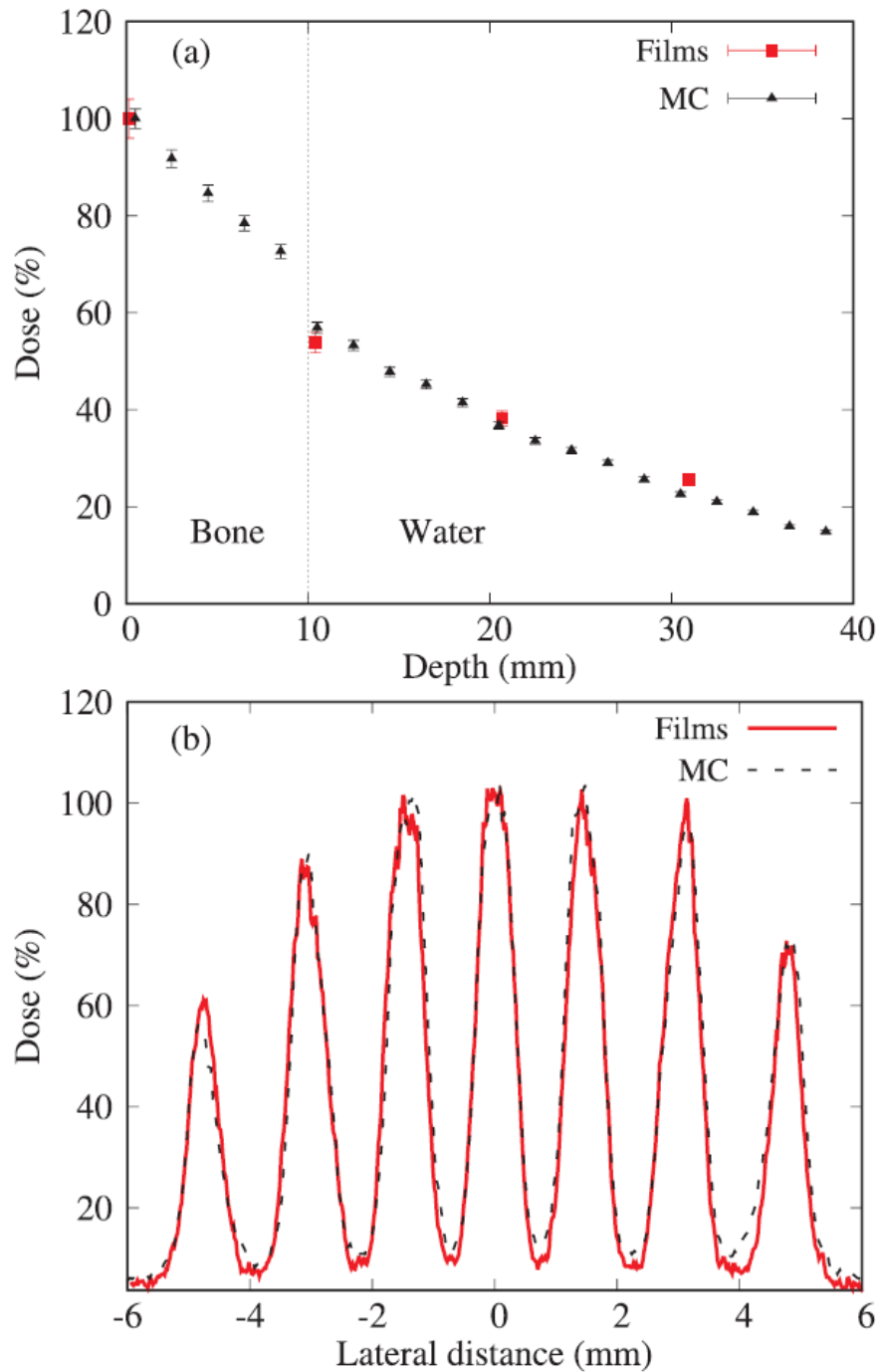


180

181 *Fig. 3: Full width at half maximum of the central peak, comparison between experimental (red square) and MC (black triangles).*

182 A good agreement is observed between MC and experimental data. The FWHM at the entrance is $618 \pm$
 183 $18 \mu\text{m}$, equal to the one at synchrotrons, $630 \pm 50 \mu\text{m}$ [1], within the uncertainty bars. Due to the large
 184 divergence, the FWHM will increase up to $1000 \mu\text{m}$ at 40 mm of depth, in contrast to synchrotrons, where
 185 the FWHM stays almost constant as a function of depth.

186 The MC beam patterns reproduce well the experimental values in both the homogeneous [6] and
 187 heterogeneous phantoms (see Fig. 4 (a) and 4 (b), respectively)), according to the criteria explained in the
 188 TRS430 [9]. At a depth of 30 mm, the differences reach the critical value of 3% (see Fig. 4 (a)). However, at
 189 this depth, this is already outside the head of the animal (see Fig. 6). The centre-to-centre (ctc) values
 190 between the three central peaks at a depth of 10 mm are $1465 \pm 10 \mu\text{m}$ and $1478 \pm 15 \mu\text{m}$ for experimental
 191 and MC respectively.



192

193 *Fig. 4: Dose distributions in the heterogeneous phantoms (bone 10 mm + water), comparison between experimental (red square)*
 194 *and Monte Carlo (black triangles) dosimetry. Percentage depth dose, panel (a) and lateral dose profiles at 10 mm of depth, panel*
 195 *(b). The values were normalized to the maximum value of the central peak.*

196 Table 1 compares the PVDR values at the ESRF [2] with the ones obtained in this research. The
 197 experimental and calculated values are in agreement. In both the synchrotron and SARRP systems, the
 198 PVDRs in the entrance are very high. The PVDR then decrease. But, while the PVDR remain constant as a

199 function of depth in the case of the synchrotron, a continuous decrease is observed in the SARRP due to
 200 the significant beam divergence.

201 *Table 1: PVDR at different depths obtained experimentally from synchrotron [2] and experimentally using Gafchromic films and*
 202 *MC simulations in this research. The acronyms are as follows: this-w-ho: This work, homogeneous phantom and this-w-he: This*
 203 *work, heterogenous phantom.*

Depth (mm)	Sync-MBRT film	this-w-ho [6] film	this-w-ho MC	this-w-he film	this-w-he MC
Surface	21.7 ± 2.2	27.8 ± 2.8	25.4 ± 1.3	24.5 ± 1.4	24.3 ± 1.5
10	17.5 ± 1.8	12.4 ± 2.3	11.6 ± 0.9	10.1 ± 0.7	9.1 ± 0.6
20	16.1 ± 1.6	9.4 ± 2.0	7.8 ± 0.5	7.1 ± 0.6	6.2 ± 0.4
30	15.6 ± 1.6	7.0 ± 1.8	5.4 ± 0.3	5.7 ± 0.5	5.2 ± 0.3

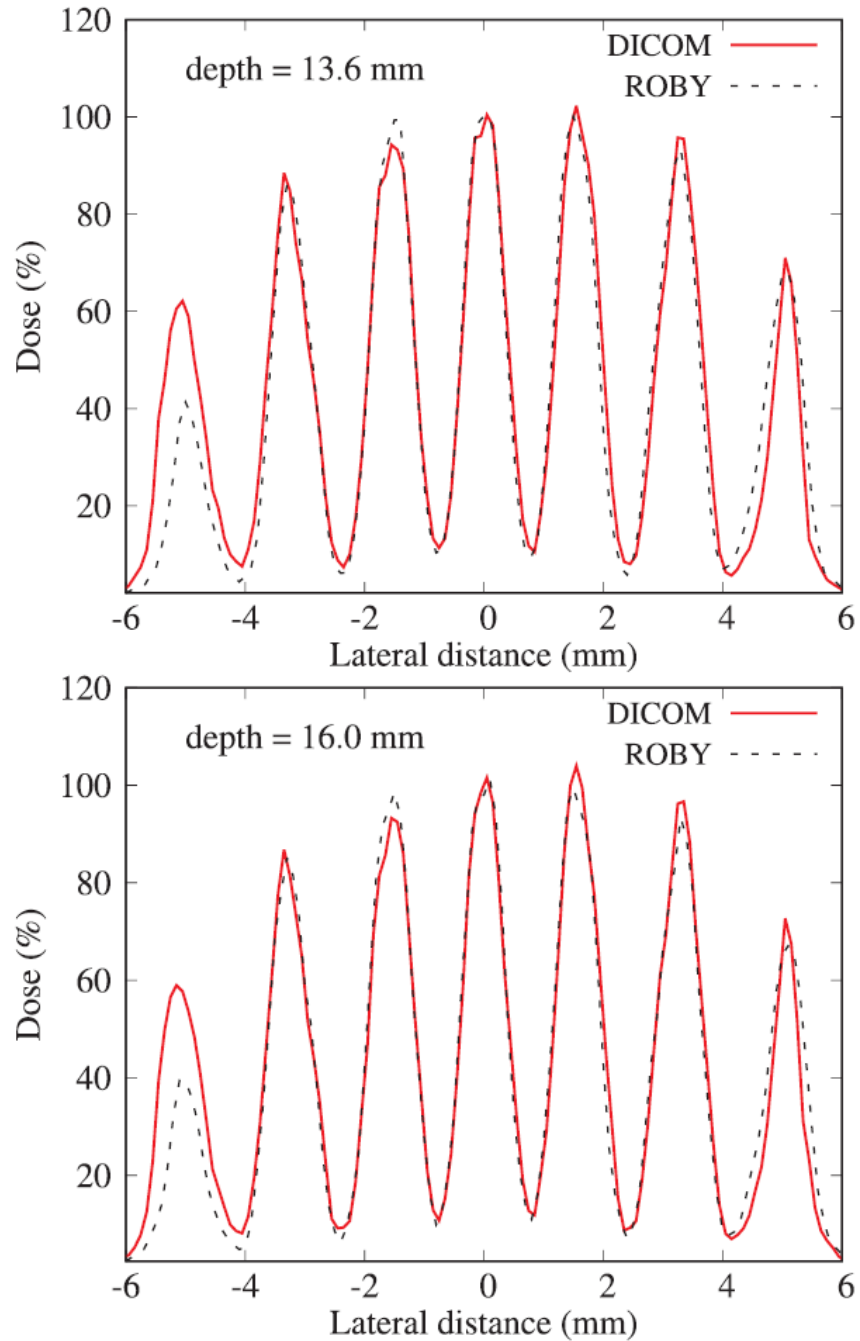
204
 205 The output factors (OF) for the central peak were calculated with respect to the broad beam (40 × 40 mm²
 206 field size). Table 2 shows the experimental and theoretical values of the OF. A good agreement is also
 207 found. The OF decrease by a factor of 3 when moving from the entrance to a depth of 3 cm. That is to say,
 208 at the surface the dose deposited by the central peak of the array is 9% lower than the one deposited by
 209 a 40×40 mm² field size, while at a depth of 3 cm, the dose in the peak is 67% lower than in broad beam
 210 conditions, due to lateral scattering and beam divergence.

211 *Table 2: Output factors obtained experimentally by using Gafchromic films and theoretically by MC simulations.*

Depth (mm)	OF (film)	OF (MC)
Surface	0.91 ± 0.04	0.92 ± 0.08
10	0.62 ± 0.02	0.63 ± 0.05
20	0.45 ± 0.02	0.47 ± 0.03
30	0.33 ± 0.01	0.35 ± 0.02

212
 213 The validated dose-engine was employed to calculate the dose distributions in the voxelized rat phantoms
 214 with the objective of planning the in vivo experiment. First of all, the dose-engine was calibrated. The
 215 experimental dose at a depth of 10 mm in the solid water phantom was compared with the calculated
 216 dose at the same depth (reference dosimetry conditions). Taking into account the number of primary
 217 particles in the simulation, a correlation of the dose at the centre of the rat can be established with respect
 218 to the dose at the reference conditions. The latter amounted to 66% ± 1% of the dose at the reference
 219 conditions.

220 The dose distribution profiles at the centre of the rat brain (13.6 mm depth) and at the tumor location
 221 (16 mm depth) were compared between CT and ROBY phantoms, see Fig. 5.



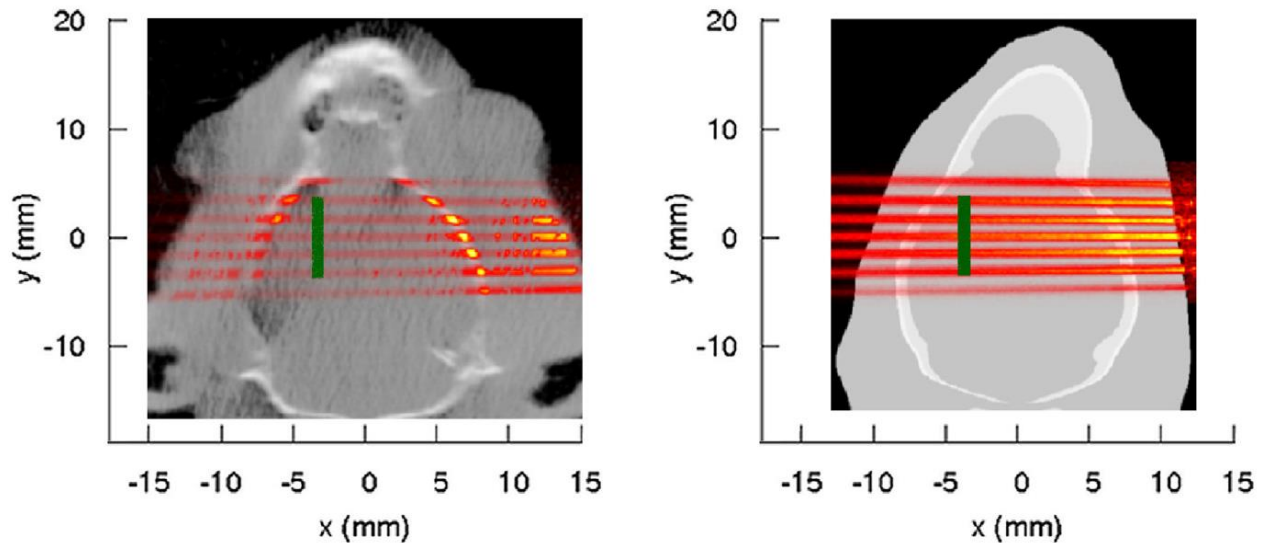
222

223
224

Fig. 5: Lateral dose profiles at the centre of the rat brain (13.6 mm depth, left panel) and at the position of the tumor (16 mm depth, right panel). The values were normalized to the maximum value of the central peak.

225

A good match was reached except that differences of up to 20% are obtained in the most extreme peak (-
226 5 mm in the y axis Figs. 5 and 6) where the thickness of the bone in the ROBY phantom is almost 2 mm in
227 contrast to 1 mm in the CT.



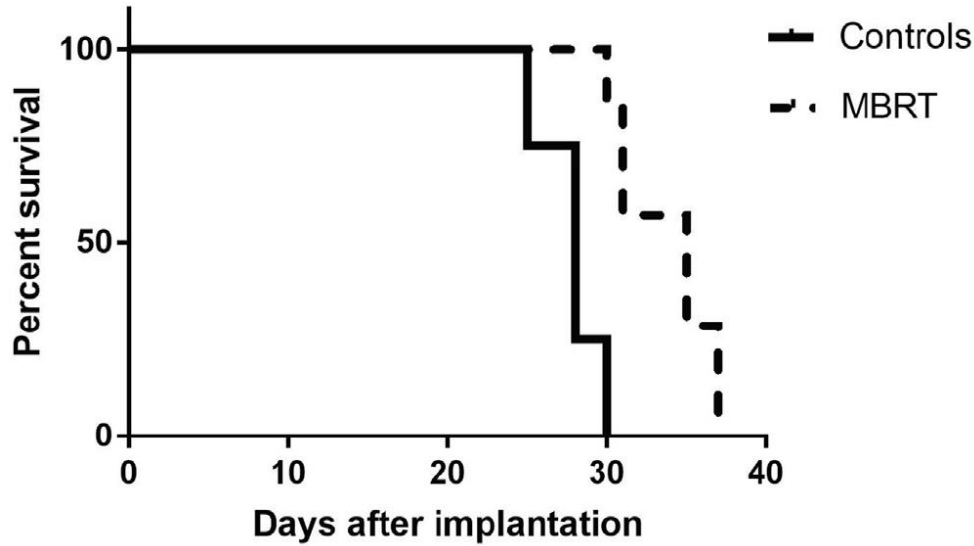
228

229 *Fig. 6: Coronal view of the dose distributions overlapped with the mass density maps for a CT slice (left panel) and for a ROBY*
 230 *slice (right panel). The location of the tumor is represented by a green line.*

231 Using the ROBY phantom, it is not necessary to make a CT scan for each animal for planning purposes,
 232 which leads to economic savings, since it is possible to adapt the parameters of the ROBY phantom taking
 233 into account the age of the animal. The PVDR values obtained for the CT and ROBY at a depth of 13.6 mm
 234 were 9.0 ± 1.3 and 9.2 ± 1.2 respectively and at a depth of 16 mm, they were 8.2 ± 1.3 and 8.5 ± 1.2
 235 respectively. These values were used to estimate the doses at the centre and at the location of the tumor.
 236 The doses calculated using the dose-engine program at the approximate centre of the tumor (16 mm
 237 depth) were 33.2 ± 1.7 Gy and 4.0 ± 0.4 Gy, peak and valley, respectively, when the CT images are used
 238 and 34.2 ± 1.7 Gy and 4.0 ± 0.4 Gy, peak and valley doses, when using the ROBY phantom. The average
 239 dose at a depth of 16 mm was 14.2 ± 0.9 Gy and 13.6 ± 0.8 Gy, in the CT and ROBY, respectively.

240 b. In vivo experiment

241 Fig. 7 shows the survival curve obtained in the in vivo experiment with the male Fisher rats. The median
 242 survival time post-implantation was calculated (28 days for the controls versus 35 days for the irradiated
 243 animals). Kaplan Meier survival data were plotted versus time after tumor implantation. The survival
 244 curves were compared using the log-rank test between the irradiated group and the controls (Prism-
 245 GraphPad). The two curves are statistically significantly different ($p = 0.0017$). The histological analysis
 246 confirmed the presence of tumors in all animals.



247

248 *Fig. 7: Survival curves of the control and irradiated groups. MBRT treatment resulted in a statistically significant but modest*
 249 *increase of mean survival time with respect to the untreated controls.*

250 IV. DISCUSSION

251 Minibeam radiation therapy is a promising radiotherapy technique whose advancement has been
 252 hindered due to the limited beamtime access at large synchrotrons. We have recently shown the feasibility
 253 of transferring this technique to a small-animal irradiator [6]. In contrast to some other work [18,19], our
 254 implementation allows the irradiation of intracranial tumors in rodents, as has been shown in the present
 255 technical note. Therefore, our system offers the possibility of performing systematic and comprehensive
 256 radiobiological experiments to investigate the distinct biological effects that occur when a spatial
 257 fractionation of the dose is used.

258 To guide such experiments, reliable dosimetry tools are needed to be able to extract valid conclusions.
 259 This includes a dose-calculation engine. With that aim, we have performed a series of experimental
 260 measurements both in homogeneous and heterogeneous dose phantoms. These measurements confirm
 261 that our beam patterns are similar to those at synchrotrons: similar beam widths, ctc distances and PVDR
 262 were obtained. In addition, they served to benchmark the preclinical dose-calculation engine that we have
 263 developed. To gain in calculation efficiency, we determined a virtual source model, that was subsequently
 264 used as beam source in the dose-calculation engine.

265 Finally, we have used the developed tools to evaluate the dose distributions delivered to a series of F98
 266 tumor-bearing rats. Unlike other MBRT table-top solutions [18,19], our system allows the irradiation of
 267 intracranial tumors in rodents, as has been shown in the present technical note. Following our previous
 268 paper [6], demonstrating that normal rats do not exhibit any important brain damage after an MBRT

269 irradiation with a 58 Gy peak dose, the pilot experiment reported here aimed at assessing whether this
270 dose prescription was also enough to achieve some tumor response. A modest but statistically significant
271 increase of mean survival time was observed in the treated group with respect to the controls. No
272 comparison was possible with standard broad beam conditions, as the prescribed dose would not have
273 been well tolerated [6].

274 V. CONCLUSIONS

275 This technical note reports on the dosimetric tools that we have developed to reliably guide preclinical
276 trials in a table-top MBRT system. As a proof of concept, we have performed a pilot experiment of the
277 treatment of intracranial glioma-bearing rats. The increase in mean survival life due to the treatment of
278 intracranial glioma-bearing rats is small but statistically significant. However, the fact that normal tissues
279 are able to withstand the high doses employed in this study, in contrast to conventional irradiation, opens
280 the possibility of escalating the dose in the tumor and the use of interlaced or cross-fired geometries to
281 improve the treatment's outcome.

282

283 Acknowledgments

284 This research was performed with financial support from ITMO Cancer AVIESAN (Alliance Nationale pour
285 les Sciences de la Vie et de la Santé, National Alliance for Life Sciences and Health) within the framework
286 of the Cancer Plan (2009–2013), under grant agreement PC201327. The authors acknowledge the
287 calculation time provided at Centre de Calcul de Lyon (IN2P3), at Grand Equipement National de Calcul
288 Intensif (in particular at the supercomputer Curie of CEA) and PRACE for awarding us access to the
289 MareNostrum computational cluster at BSC (Spain) under grant agreement number 2016153507.

290

291 References

- 292 [1] Prezado Y, Renier M, Bravin A. A new method of creating minibeam patterns for synchrotron
293 radiation therapy: a feasibility study. *J Synchr Radiat* 2009;16:582–6.
- 294 [2] Prezado Y, et al. Dosimetry protocol for the preclinical trials in white-beam minibeam radiation
295 therapy. *Med Phys* 2011;38:5012–20.
- 296 [3] Dilmanian FA, Button TM, et al. Response of rat intracranial 9L gliosarcoma to microbeam radiation
297 therapy. *Neuro Oncol* 2002;4:26–38.
- 298 [4] Prezado Y, Deman P, et al. Tolerance dose escalation in minibeam radiation therapy applied to
299 normal rat brain: long-term clinical, radiological and histopathological analysis. *Rad Res* 2015;184.
300 314-2.

- 301 [5] Prezado Y, Sarun S, et al. Increase of lifespan for glioma-bearing rats by using minibeam radiation
302 therapy. *J Synchr Radiat* 2012;19:60–5.
- 303 [6] Prezado Y, dos Santos M, González W, et al. Transfer of Minibeam Radiation Therapy into a cost-
304 effective equipment for radiobiological studies: a proof of concept. *Sci Rep* 2017;7:17295.
- 305 [7] URL: <http://www.xstrahl.com/>.
- 306 [8] Agostinelli S, et al. Geant4 a simulation toolkit. *NIM A* 2003;506:250–303.
- 307 [9] International Atomic Energy Agency 2004 Commissioning and quality assurance of computerized
308 planning systems for radiation treatment of cancer IAEA Technical. Report Series 430 (Vienna:
309 IAEA), 2004.
- 310 [10] URL: http://www.sunnuclear.com/solutions/machineqa/solid_water_he.
- 311 [11] Keenan MA, et al. RADAR realistic animal model series for dose assessment. *J Nucl Med*
312 2010;51:471–6.
- 313 [12] Hamdia M, et al. Impact of X-ray energy on absorbed dose assessed with Monte Carlo simulations
314 in a mouse tumor and in nearest organs irradiated with kilovoltage X-ray beams. *Cancer Radiother*
315 2017;21:190–8.
- 316 [13] Reynaert N, et al. Monte Carlo treatment planning for photon and electron beams. *Radiat Phys*
317 *Chem* 2007;76:643–86.
- 318 [14] Devic S, et al. Precise radiochromic film dosimetry using flat-bed document scanner. *Med Phys*
319 2005;32:2245–53.
- 320 [15] Niroomand-Rad A, et al. Radiochromic film dosimetry: recommendations of AAPM radiation
321 therapy committee task group 55. *Med Phys* 1998;25:2093–115.
- 322 [16] Sorriaux J, et al. Evaluation of Gafchromic EBT3 films characteristics in therapy photon, electron
323 and proton beams. *Phys Med* 2013;29:599–606.
- 324 [17] Prezado Y, et al. Proton minibeam radiation therapy widens the therapeutic index for high-grade
325 gliomas. *Sci Rep* 2018;8:16479.
- 326 [18] Bartzsch S, et al. preclinical microbeam facility with a conventional x-ray tube. *Med Phys*
327 2016;43:6301–8.
- 328 [19] Bazyar S, et al. Minibeam radiotherapy with small animal irradiators; In vitro and in vivo feasibility
329 studies. *Phys Med Biol* 2017;62:8924–42.

330